ADVANCED OPTICAL MATERIALS
www.advopticalmat.de

Metasurface-Based Free-Space Multi-Port Beam Splitter with Arbitrary Power Ratio

Tian Tian, Yuxuan Liao, Xue Feng, Kaiyu Cui, Fang Liu, Wei Zhang, and Yidong Huang**

A beam splitter (BS) is one of the most critical building blocks in optical systems. Despite various attempts of flat-type BSs to miniaturize the conventional cube BS reported, it remains a challenge to realize an ultrathin optical BS with multi-port output, non-uniform splitting ratio, and steerable outgoing directions. Herein, a free-space optical multi-port beam splitter (MPBS) based on a polarization-independent all-dielectric metasurface is demonstrated. By applying an optimized phase-pattern paradigm via a gradient-descent-based iterative algorithm to amorphous silicon (α-Si) metasurfaces, a variety of MPBS samples with arbitrarily predetermined output port number (2–7), power ratio, and spatial distribution of output beams are prepared. The experimental results reveal that the fabricated MPBSs can achieve high total splitting efficiency (TSE, above 74.7%) and beam-splitting fidelity (similarity, above 78.4%) within the bandwidth of 100 nm (1500–1600 nm). Such proposed MPBS can provide fabulous flexibility for optical integrated system and diverse applications.

1. Introduction

A beam splitter (BS), which could distribute and combine the optical beam paths, serves as one of the most fundamental building blocks in a variety of optical systems. Typically, the most common BS divides the incident light beam into two output channels (denoted as 2-port BS). Such 2-port BS plays a significant role in diverse optical applications of interferometers,[1,2] spectroscopy,[3] optical communications,[4] etc. Previously, the conventional 2-port BS has been intensively investigated in both free-space (e.g., the cube BS[5]) and on-chip (e.g., y-branch waveguide,[6,7] directional coupler[8]) optical systems. Nevertheless, the cube BS is hard to be integrated on-chip since the optical path relies on the birefringence of the bulky prisms. As more compact alternatives, some flat-type BSs (e.g., grating BS,[9] dichroic BS[10]) have been recently demonstrated. Besides the traditional 2-port BSs, we have noticed that for some specific applications, e.g., light detection and ranging (LiDAR),[11] beamforming networks,[12] quantum optics[13] and optical computing,[14,15] a multi-port beam splitter (MPBS) is highly desired. The functionality of the MPBS is to distribute the incident beam into N (N>2) output channels with predetermined power ratio. Furthermore, for these applications, the operation wavelength and polarization should keep constant since the optical interference can be employed to perform some processing or calculation in optical domain. Such a MPBS is actually very difficult to achieve through traditional methods in both free-space and integrated systems since both the wavelength and polarization cannot be utilized to guide the optical beam. For instance, the widely used multimode interference (MMI) coupler only can divide the incident beam into N output channels with uniform power ratio.[16,17] Another scheme is the multi-port interferometer, which is constructed by a specific mesh of 2×2 BSs and phase shifters.[18] Since such N-port interferometer requires cascaded N×(N-1) 2-port BSs, it is still challenging to fabricate and not cost-efficient. One promising method to achieve an optical MPBS with a single compact element is to employ the burgeoning metasurface.

Metasurface is a 2D artificial structure with periodic arrangement of subwavelength scattering unit cells, which are referred to as "meta-atoms". During the past decades, metasurface has attracted extensive attentions owing to its overwhelming superiority over conventional optical components.[19,20] Specifically, as a compact planar structure, metasurface meets the incremental pursuit of photonic integrated systems to miniaturize the footprint. Furthermore, with different materials (e.g., dielectric,[21,22] metal[23,24]) and geometric structure of unit cells,[25,26] it is flexible to design metasurface-empowered devices with the operation frequency band ranging from visible,[27-29] terahertz,[30] to microwave.[31] Notably, metasurface also exhibits the unprecedented capability to manipulate the electromagnetic wave in various degrees of freedom including phase,[32-34] amplitude[35,36] and polarization.[37] By taking advantage of these intriguing properties, metasurface could extend the functionalities of existing optical components and further achieve novel devices. For instance, the exceptional wavefront engineering capability endowed by metasurface has been widely investigated including metalenses,[38,39] abnormal reflection,[32] negative refraction,[40] vortex beam generation,[41] meta-holography[42] and dynamic beam steering devices.[43] Moreover, metasurface is also employed to demonstrate various novel devices such as perfect

T. Tian, Y. Liao, X. Feng, K. Cui, F. Liu, W. Zhang, Y. Huang
Department of Electronic Engineering
Tsinghua University
Beijing 100084, China
E-mail: x-feng@tsinghua.edu.cn; yidonghuang@tsinghua.edu.cn

The ORCID identification number(s) for the author(s) of this article can be found under https://doi.org/10.1002/adom.202300664

DOI: 10.1002/adom.202300664

absorbers,[44] invisibility skin cloak,[45] optical isolator[46] and color printer.[47] Based on metasurfaces, several optical 2-port BSs[48-52] have recently been demonstrated with ultra-compact size ($33.6 \times 33.6\ \mu m^2$ as a concrete example[48]), which are very promising to replace the conventional cube BSs. In these work, only a few theoretical proposals realized the asymmetric (i.e., non-identical splitting angle or non-uniform power ratio) BSs based on the difference of incident angle[49] or frequency,[52] even by altering the refractive index of the substrate.[48] As mentioned above, for our considering MPBS, the wavelength and polarization cannot be utilized to separate the light beam as well as the incident angle since the incident beam is constant. Thus, the metasurface is the most promising candidate through the controllable transmission phase distribution within the transverse plane.

In this work, we have proposed and demonstrated a free-space optical MPBS with arbitrarily predetermined port number, power ratio and spatial distribution of output beams for a single wavelength input beam. The MPBS is fabricated on the amorphous silicon (α-Si) metasurface and due to the geometry of utilized nanopillar, non-polarizing operation is also achieved. With our proposal, it should be mentioned that the propagating direction and transverse mode profiles of the input and output beams are maintained, which would be convenient for cascading and cooperating with other elements in optical systems. Specifically, the operation mechanism of the proposed MPBS is based on a complex grating-like diffraction phase pattern optimized by a gradient-descent-based iterative algorithm. As a proof of concept, we have applied the optimized phase-grating paradigm on elaborately designed α-Si metasurfaces and fabricated different MPBS samples with various port number ($N = 2$–7), power ratio and spatial distributions. To evaluate the performance, two parameters of total splitting efficiency (TSE) and beam-splitting ratio similarity are employed to characterize the efficiency and fidelity of fabricated samples. According to the experimental results, the TSE and similarity are 74.7%–80.7% and 78.4%–89.3% within the wavelength range of 1500–1600 nm, respectively. To the best of our knowledge, this work is the first demonstration of optical multi-port beam splitting. Compared with previous metasurface-based 2-port BSs, our proposed MPBS not only demonstrates multi-port beam-splitting successfully, but also achieves arbitrary power ratio along with arbitrarily predetermined port number and the spatial distribution of output beams, which relies on the powerful capabilities of metasurface on wavefront shaping and optical steering. We believe that such proposed MPBS would boost up to exploit the applications of BSs by a large margin.

2. Results and Discussion

2.1. Design Methods

The functionality of our proposed free-space MPBS is to split the incident single wavelength light beam into multiple sub-beams with respectively predetermined power (denoted as normalized $P_1 \sim P_N$) while the operation wavelength and polarization keep constant. With our proposal, an arbitrary MPBS can be readily achieved once the port number, splitting ratio as well as the spatial distributions of the output beams are specified. As a concrete example, **Figure 1a** shows the schematic of a 5-port BS, in which the input light beam illuminates on the MPBS and splits into five sub-beams with predetermined power ratio of $P_1:P_2:P_3:P_4:P_5 = 1:2:3:4:5$. After propagating a certain distance along the respectively distinct deflecting direction, the sub-beams are received on the observation plane and defined as the output ports of the device. Here, for the specific case in Figure 1b, the spatial distribution of the output beams is considered as equally spaced on a circle of the received plane.

A diffraction grating is the simplest structure to perform beam splitting. However, a single grating cannot split the incident beam into multiple output beams with non-uniform power ratio. Actually, a series of gratings are required to perform the task of multi-port beam splitting. Thanks to the distinctive wavefront control capability, a 2D complex grating-like diffraction phase pattern can be achieved by the phase-gradient metasurface. Hence, the process to design a metasurface-based MPBS can be considered as two steps. The first step is to design a proper diffraction phase pattern to achieve the desired multi-port beam splitting and the second step is to determine the distribution of "meta-atoms" corresponding to the phase pattern acquired in first step. In the following text, we will consider a 5-port BS shown in Figure 1b as a specific example to introduce the design process in detail.

Firstly, both the incident and output beam are considered as the same transverse mode profile. Theoretically, the MPBS is independent of the mode of both the input and output. In this work, the mode profile is specifically set as fundamental Gaussian mode since it is commonly utilized in most spatial optical systems. Besides, in our design, the number and the spatial distribution of the output ports can be flexibly settled. The only restriction is to avoid the overlap between adjacent output beams, which is corresponding to the divergence angle of the Gaussian beam, the angle of beam deflecting and the distance between the incident and the observation plane. Here, the case shown in Figure 1b is set as a specific circumstance. The incident beam, which is a Gaussian-mode with a beam waist radius of 40 μm, falls precisely on the MPBS and then splits into five sub-beams with the same deflecting angle of 4.1°. After a propagation distance of 6 mm, the output beams are received by an observation plane, representing uniformly distributed around a 430 μm-radius circle (see Supporting Information for detailed discussions about the size of beam waist). Following these settled parameters, a diffraction phase pattern could be determined.

Before focusing on the concrete example, we should first determine how to design a diffraction phase pattern to deflect the incident wave to distinct outgoing directions at the same time. A straightforward but effective recipe is to utilize superposed phase gratings. It has been recently demonstrated that a mixed phase pattern will simultaneously perform respective phase compensation according to the superposition theorem.[53] As shown in Figure 1b, for convenience, the center of the incident light beam is considered as the origin of the coordinate and then the diffraction pattern composed of a series of blazed gratings can be expressed as:

$$F_1(\mathbf{r}) = \arg\{\sum_{n=1}^{N} A_n \exp\left[-i\mathbf{k}_n \cdot (\mathbf{r} - \mathbf{R}_n)\right]\} \quad (1)$$

where N refers to the number of the output ports, and A_n indicates the normalized amplitude of the n_{th} sub-beam.

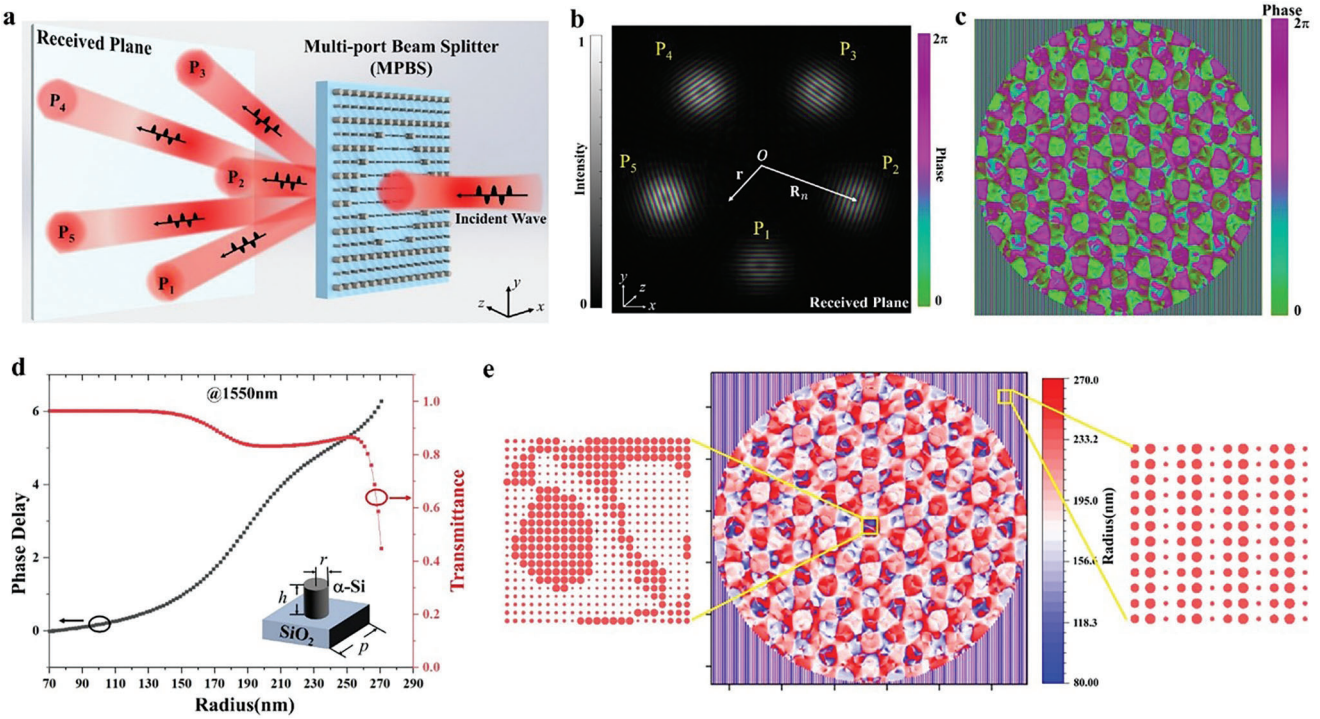

Figure 1. The schemes and design process for the metasurface-based free-space optical MPBS. a) The schematic of a 5-port BS example with power ratio of P_1:P_2:P_3:P_4:P_5. b) The desired output on the received plane of the 5-port BS with power ratio of P_1:P_2:P_3:P_4:P_5 = 1:2:3:4:5. The brightness reveals the light intensity values while the color indicates the phase values of sub-beams. c)The optimized phase-only pattern obtained by gradient-descent-based algorithm for the 5-port beam splitting with power ratio of 1:2:3:4:5. d) The simulated phase delay and transmittance versus the varied radius (70–270 nm) of α-Si nano-pillars. Through systematically sweeping the parameters, the carefully selected height and period of the nanopillars are h = 750 and p = 630 nm, respectively. e) The whole and partial arrangement diagrams of nano-pillar radius for the metasurface-based MPBS with power ratio of 1:2:3:4:5.

Displacement vector $\boldsymbol{r}$ and $\boldsymbol{R}_n$ are the position coordinates of a certain point and the central point of the n_{th} output beam on the transverse plane, respectively.$\mathbf{k}^n = (\mathbf{k}_x^n, \mathbf{k}_y^n)$represents the corresponding transverse wave vector compensation of the n_{th} sub-beam deflected from the incident beam, resulting in the deflection angle of $tan^{-1}(\mathbf{k}_x^n/\mathbf{k})$ and $tan^{-1}(\mathbf{k}_y^n/\mathbf{k})$ along x-axis and y-axis, respectively. Besides, considering the circular symmetric distribution on the transverse plane of the Gaussian beam, the functional area of diffraction pattern contributing by Equation 1 is purposely set as a circular region to match the incident beam. The Equation 1 is rewritten as:

$$F_2(\mathbf{r}) = F_1(\mathbf{r}) \times \chi(\mathbf{r}), \chi(\mathbf{r}) = \begin{cases} 1, & |\mathbf{r}| < R_{threshold} \\ 0, & otherwise \end{cases} \quad (2)$$

where, $R_{threshold}$ is determined by the beam waist of the incident Gaussian spot.

Additionally, to spatially filter out the undesired light, a three-step diffraction grating is additionally implemented in the surrounding area, which is given by $F_{grating}(\boldsymbol{r}) = \exp(i\boldsymbol{k}_{grating} \cdot \boldsymbol{r})$.

Thus, the ultimate diffraction phase pattern is expressed as:

$$F(\mathbf{r}) = \arg\{\sum_{n=1}^{N} A_n \exp\left[-i\mathbf{k}_n \cdot (\mathbf{r} - \mathbf{R}_n)\right]\} \times \chi(\mathbf{r}) + \exp(i\mathbf{k}_{grating} \cdot \mathbf{r}) \quad (3)$$

However, the phase-only modulation induced by phase gratings cannot accurately accomplish the arbitrary power ratio beam splitting functionality, which involves both the amplitude and phase information. Thus, an iterative algorithm with gradient descent is employed to obtain the optimal phase-only pattern, which produces the light field distribution on the target plane to approximate an ideal distribution. The main procedure to generate the optimized phase pattern and the light field simulation method based on Discrete Fourier Transform (DFT) can be found in Figure S1,2 (Supporting Information). Figure 1c is the finally optimized two-dimensional diffraction pattern to perform the 5-port beam splitting with power ratio of 1:2:3:4:5, which is comprised of the complex phase pattern in the circular area to generate target light field and the stripe pattern in the surrounding area to filter out the undesired beams. Compared with the diffraction pattern given by Equation 3, the optimized one contains more meticulous details, promising more accurate target light field (Figure S3, Supporting Information). It should be mentioned that our utilized iterative algorithm with gradient descent is a backward optimization algorithm. Thus it is different from the greyscale computer-generated holography (CGH) algorithm, which is a kind of forward simulation method (see Supporting Information for detailed discussions). Besides, we have deduced the complex-number form of this optimization. This complex algorithm can make more effective use of the computing library than the real number algorithm, so it can obtain the results with

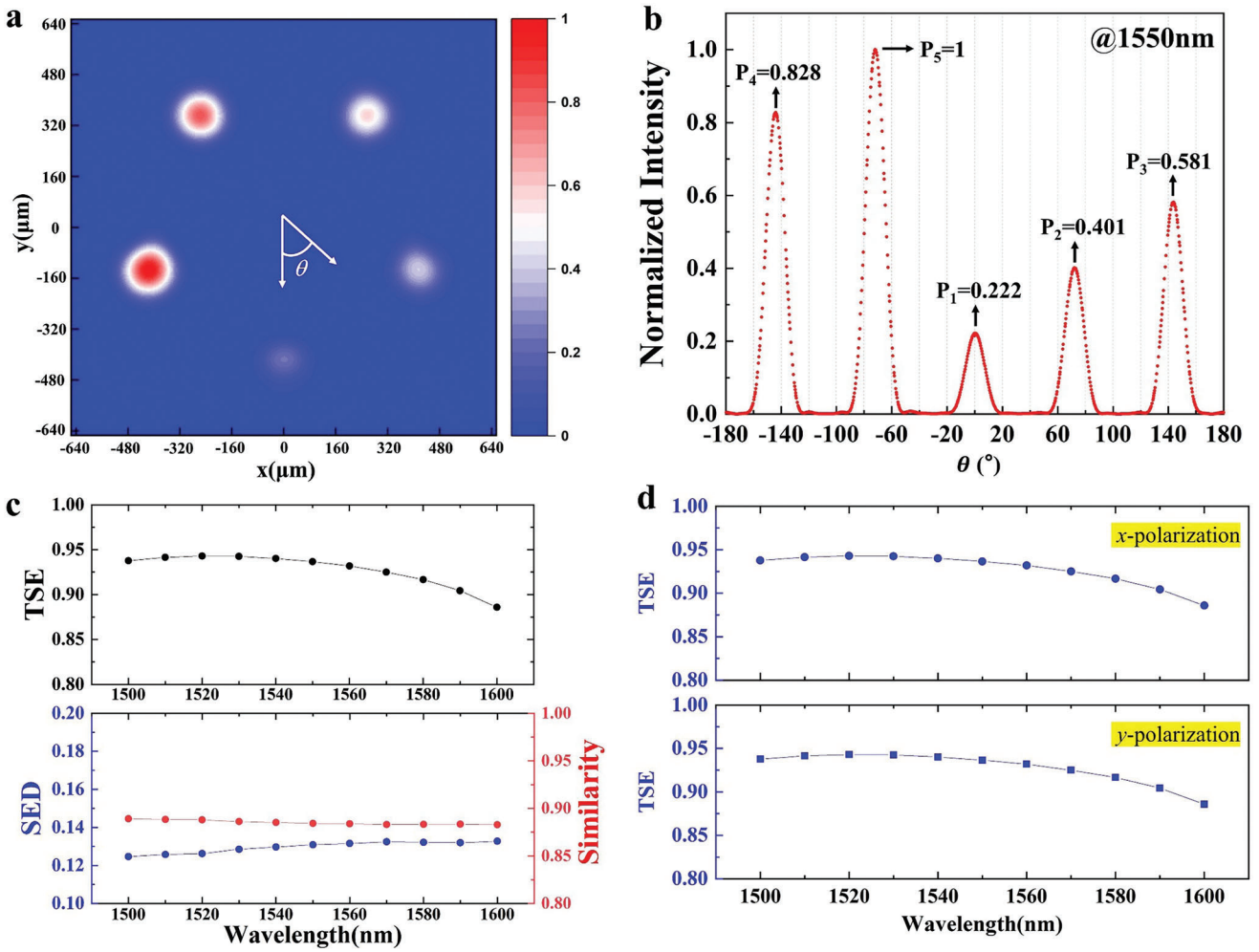

Figure 2. Simulation results of the proposed MPBS with power ratio of 1:2:3:4:5. a) The output beams with normalized light intensity on the received plane. b) The extracted normalized peak power ratio of each sub-beams versus the azimuth angle θ, θ is defined as the polar angle with negative y-axis on the received plane, as shown in (a). c) The calculated TSE and SED (similarity) in the wavelength range of 1500–1600 nm with wavelength interval of 10 nm. d) The TSE for the *x*-polarization and *y*-polarization incident light.

much faster speed. Moreover, the optimization complexity of our utilized algorithm is independent on the number of ports, but only depends on the area and resolution of the optimization region (i.e., the total number of pixels). In this work, the optimization is running with MATLAB and a GTX 1660Ti GPU is used, and the resolution is 2048 by 2048. It takes just a few seconds to optimize a hologram.

After obtaining the phase pattern, we further apply the optimized phase-grating paradigm on an elaborately designed metasurface. Here, the metasurface is considered as α-Si nano-pillar array on quartz substrate to achieve polarization independent operation. For more accuracy, we first measured the dielectric function of α-Si sample deposited on 300 μm quartz substrate by plasma enhanced chemical vapor deposition (PECVD) by spectroscopic ellipsometry. The details are provided in Figure S6 (Supporting Information). Typically, with the measured refractive index ($n = 3.324$) and absorption coefficient ($k = 0.015$) at the wavelength of 1550 nm, the phase delay and transmittance have been calculated by Finite-Difference-Time-Domain (FDTD) method within the radius range of 70–270 nm. The lattice constant and height of the nano-pillars have been carefully selected so that the phase delay can be nearly regulated from 0 to 2π and high transmission efficiency can be maintained simultaneously (Figure 1d). With the relation between the phase delay and the radius of the nano-pillars, the proper arrangement of nano-pillar radius (Figure 1e) can be obtained to construct the MPBS.

2.2. Simulation Results

To verify our design shown in Figure 1e, some FDTD simulations have been carried out. Actually, due to the limited computing capacity of the simulations, the MPBS has a more compact size of 90 × 90 μm^2, i.e., 143 × 143 α-Si nano-pillars involved in the simulation, and it is illuminated by an *x*-polarization Gaussian incident light with the radius of beam waist as 40 μm. **Figure 2a** shows the simulation result of the MPBS with predesigned power ratio of 1:2:3:4:5. Figure 2b shows the power distribution versus

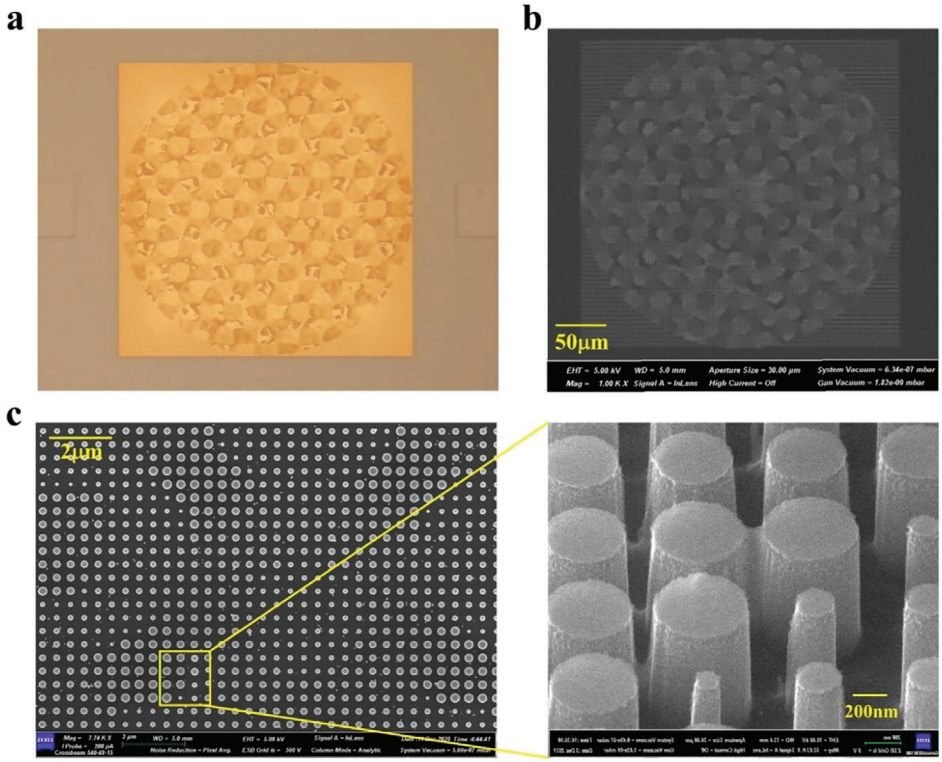

Figure 3. The optical microscope image and SEM images of the fabricated sample with splitting ratio of P_1:P_2:P_3:P_4:P_5 = 1:2:3:4:5. a) The optical microscope image of the MPBS sample. b) The overall SEM image of the MPBS sample. c) The partially enlarged SEM images of the MPBS sample.

the azimuth angle θ and the peak power ratio of each sub-beam. It can be seen that the beam splitting ratio is quite consistent with the theoretical design.

Additionally, to evaluate the performance of the MPBS, two parameters are employed. The first one is the total splitting efficiency (TSE), which is the ratio of the total intensity of the desired sub-beams to the total intensity of all transmitted light and expressed by Equation 4. The other one is standardized Euclidean distance (SED),[54] which evaluates the discrepancy of the theoretical splitting ratio vector and the experimental one. In addition, similarity is also introduced to characterize the beam-splitting fidelity more clearly. The relation between SED and similarity is expressed as Equation 5. As shown in Figure 2c, the simulated TSE can reach >88% with similarity >88.2% (SED<0.133) in the wavelength range of 1500–1600 nm, which covers the C-band and most of L-band. Besides, to demonstrate the polarization independence of the MPBS, we have repeated the simulations with y-polarization Gaussian incident light and plot the results in Figure 2d. According to the simulation results of both x and y-polarization, our purposed MPBS is insensitive to the polarization states of the incident light beam.

$$TSE = \frac{\sum_{i=1}^{N} I_i}{I_{total}} \tag{4}$$

$$Similarity = \frac{1}{1 + |SED|} \tag{5}$$

2.3. Experimental Results

Further, several MPBS samples with various splitting ratio have been fabricated and measured. At first, α-Si (thickness of 750 nm) was deposited on a quartz substrate by PECVD. Then, the MPBS samples were fabricated on α-Si layer with electron beam lithography (EBL) and inductively coupled plasma reactive ion etching (ICP-RIE). It is worth mentioning that a hard mask of Cr layer was adopted to increase the aspect ratio of the nano-pillars, and an additional SiO_2 mask was also employed to avoid experimentally cumbersome lift-off process of Cr. The details of fabrication processes can be found in Figure S7 (Supporting Information), and the comparative results of fabricated samples using Cr hard mask and using bilayer mask of Cr and SiO_2 are also provided in Figure S8 (Supporting Information). **Figure 3** shows the optical microscope and scanning electron microscope (SEM) images of the fabricated sample with splitting ratio of P_1:P_2:P_3:P_4:P_5 = 1:2:3:4:5. All samples (five types of MPBSs) are comprised of 500×500 nano-pillars with size of 315×315 μm^2, which is comparable to the diameter of the incident light spot (≈300 μm) located on the MPBS bracket. Actually, such sample size is determined as a trade-off between the performance and cost. Specifically, to achieve precise beam-splitting, large area is desired so that more meta-atoms could be implemented to achieve high resolution phase pattern. However, large area sample also introduces higher cost in terms of time cost of optimizing the phase pattern and particularly the expenditure of EBL. If the standard CMOS fabrication is adopted for future mass production, the cost of implementing large area MPBS could be significantly reduced.

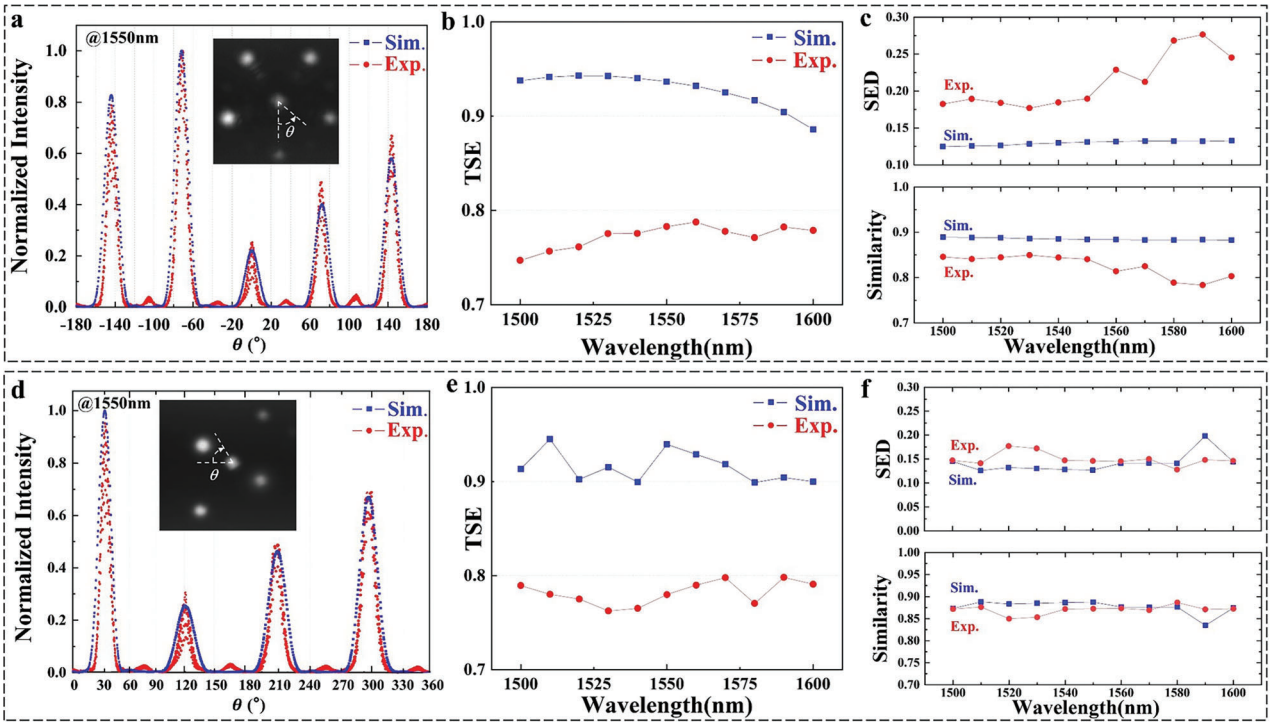

Figure 4. Experimental results of the proposed metasurface-based MPBSs with power ratio of 1:2:3:4:5 (a,b,c) and 1:2:3:4 (d,e,f). a,d) The extracted normalized peak power ratio of each sub-beams versus the azimuth angle θ, the inset shows the recorded CCD image. b,e) The simulated and experimental TSE in the wavelength range of 1500–1600 nm with wavelength interval of 10 nm. c,f) The simulated and experimental SED/similarity.

To measure the transmission of the fabricated samples, a confocal microscope system has been built up (more details are provided in Figure S9, Supporting Information). The inset image in **Figure 4a** is captured by CCD and shows a typical output of a 5-port sample with splitting ratio of 1:2:3:4:5 at the wavelength of 1550 nm. It can be seen that there is a central spot, which is the directly transmitted light without modulation and indicates that the diffraction efficiency of fabricated sample is lower than the design. The reason could be attributed to the sidewall roughness and diameter deviation of fabricated nano-pillar (detailed discussions can be found in Figure S10-13, Supporting Information). With the recorded data of CCD, the power distribution versus the azimuth angle θ can be extracted and shown in Figure 4a as red dots while the simulation results are also plotted as blue square for comparison. All results are normalized with the intensity of the maximum output beam. It can be found that the experimental results and simulations are quite consistent. Figure 4b,c show both the TSE and SED (similarity) within the operation wavelength range of 1500–1600 nm, respectively. In both figures, the results of experiment/simulation are shown as red dots/blue squares. According to the experimental results, the TSE is 74.7%–78.8% and similarity is 78.4%–85% (SED: 0.177–0.276) within the bandwidth of 100 nm, respectively. These results indicate that our proposed MPBS could operate within a very broad bandwidth. The TSE of our experiments is reasonable in the previously reported transmissive metasurface devices (discussions can be found in Table S1, Supporting Information). The polarization-independent operation of the MPBS is also measured and shown in Figure S14 (Supporting Information). Furthermore, with our proposed MPBS, the incident beam can be guided towards any direction/angle. Thus, another case with a rhombic pattern of output sub-beam spots is shown in Figure 4d–f with power ratio of 1:2:3:4. The experimental TSE is 78%–79.4% and similarity is 85%–88.7% (SED: 0.128–0.177). In addition, all the experimental results of other samples are provided in Figure S15,16 (Supporting Information) and summarized in **Table 1**. From Table 1, it can be seen that different types of free-space MPBSs, including various beam-splitting number (up to 7) and spatial distribution of output ports (circle-arranged or rhombus-arranged), have be successfully achieved.

Table 1. The complete experimental results of all fabricated samples.

Beam-Splitting Ratio	Exp.TSE	Exp.SED	Exp.similarity
1:2	76.4%–80.7%	0.13–0.175	85.1%–88.5%
1:2:3:4	78%–79.4%	0.128–0.177	85%–88.7%
1:2:3:4:5	74.7%–78.8%	0.177–0.276	78.4%–85%
1:1:1:1:1	74.7%–78.1%	0.16–0.243	80.5%–86.2%
1:1:1:1:1:1:1	77.1%–79.5%	0.12–0.175	85.1%–89.3%

3. Conclusion

In summary, we have proposed and demonstrated a free-space optical MPBS based on a polarization-independent all-dielectric metasurface. An iterative algorithm with gradient descent

optimization is utilized to design the phase grating for precisely multi-beam splitting. With such a generic optimization paradigm, a series of MPBSs have been designed and fabricated on α-Si substrate with various port number (N = 2–7), splitting ratio and spatial distributions. According to the complete experimental results of all fabricated samples, the calculated TSE and similarity are 74.7%–80.7% and 78.4%–89.3% within the bandwidth of 100 nm. Compared with previous metasurface-based 2-port BSs in visible/near-infrared regimes,[48-52] our proposed MPBS achieves multi-port beam-splitting with arbitrary power ratio, port number and the spatial distribution of output beams. This work further exhibits the flexibility of metasurface to achieve the functionalities that are hard to be obtained by conventional optical devices. Moreover, for the proposed MPBS, the characterizations of maintaining propagating directions and transverse mode profile of the incident beam are very beneficial for cascading and cooperating in expanded optical systems. We believe that such MPBS device could be promising for applications of LiDAR, beamforming networks, quantum optics and optical computing.

Supporting Information

Supporting Information is available from the Wiley Online Library or from the author.

Acknowledgements

This research was supported by the National Key Research and Development Program of China (2018YFB2200402) and the National Natural Science Foundation of China (grant no. 61875101). This work was also supported by the Beijing Academy of Quantum Information Science, Beijing National Research Center for Information Science and Technology (BNRist), Frontier Science Center for Quantum Information, Tsinghua University Initiative Scientific Research Program, and Huawei Technologies Co. Ltd. The authors would like to thank Mr. Zhiyao Ma and Prof. Yongzhuo Li for their valuable discussions and helpful comments.

Conflict of Interest

The authors declare no conflict of interest.

Author Contributions

T.T. and X.F. conceived the idea. T.T. designed and performed the simulations, experiments, and data analysis. Y.L. contributed significantly to the numerical simulations. K.C., F.L., and W.Z. provided useful discussions and comments. T.T. and X.F. wrote the paper. Y.H. revised the manuscript. The manuscript was written through contributions of all authors. All authors have given approval to the final version of the manuscript.

Data Availability Statement

The data that support the findings of this study are available from the corresponding author upon reasonable request.

Keywords

arbitrary beam-splitting ratio, diffraction phase pattern, free-space multi-port beam splitter, metasurfaces, optimization algorithm with gradient descent

Received: March 19, 2023
Revised: April 21, 2023
Published online: June 9, 2023

[1] S. Yokozeki, T. Suzuki, *Appl. Opt.* **1971**, *10*, 1575.
[2] Y. Wang, F. Xie, S. Ma, L. Dong, *Opt. Lasers Eng.* **2017**, *93*, 164.
[3] J. Bates, *Science* **1976**, *191*, 31.
[4] Wang, S. H.e, D. Dai, *Laser Photonics Rev.* **2014**, *8*, L18.
[5] F. Bassani, G. Leidl, P. Wyder, *MRS Bull.* **2006**, *31*, 192.
[6] M. Hu, J. Huang, R. Scarmozzino, M. Levy, R. Osgood, *IEEE Photonics Technol. Lett.* **1997**, *9*, 203.
[7] J. Wang, X. Guan, Y. He, Y. Shi, Z. Wang, S. He, P. Holmström, L. Wosinski, L. Thylen, D. Dai, *Opt. Express* **2011**, *19*, 838.
[8] C. Ye, D. Dai, *J. Lightwave Technol.* **2020**, *38*, 2370.
[9] J. Feng, Z. Zhou, *Opt. Lett.* **2007**, *32*, 1662.
[10] V. Karar, A. L. Sharma, *Adv. Mater.* **2017**, *2*, 398.
[11] D. Liu, C. Hostetler, I. Miller, A. Cook, J. Hair, *Opt. Express* **2012**, *20*, 1406.
[12] Y. Zhang, H. Wu, D. Zhu, S. Pan, *Opt. Express* **2014**, *22*, 3761.
[13] J. Carolan, C. Harrold, C. Sparrow, E. Martín-López, N. J. Russell, J. W. Silverstone, P. J. Shadbolt, N. Matsuda, M. Oguma, M. Itoh, *Science* **2015**, *349*, 711.
[14] M. Prabhu, C. Roques-Carmes, Y. Shen, N. Harris, L. Jing, J. Carolan, R. Hamerly, T. Baehr-Jones, M. Hochberg, V. Čeperić, *Optica* **2020**, *7*, 551.
[15] J. Spall, X. Guo, T. D. Barrett, A. Lvovsky, *Opt. Lett.* **2020**, *45*, 5752.
[16] D. Dai, Z. Wang, J. Peters, J. E. Bowers, *IEEE Photonics Technol. Lett.* **2012**, *24*, 673.
[17] S. Wang, D. Dai, *Opt. Lett.* **2018**, *43*, 2531.
[18] M. Reck, A. Zeilinger, H. J. Bernstein, P. Bertani, *Phys. Rev. Lett.* **1994**, *73*, 58.
[19] A. V. Kildishev, A. Boltasseva, V. M. Shalaev, *Science* **2013**, *339*, 1232009.
[20] W. T. Chen, A. Y. Zhu, F. Capasso, *Nat. Rev. Mater.* **2020**, *5*, 604.
[21] M. Decker, I. Staude, M. Falkner, J. Dominguez, D. N. Neshev, I. Brener, T. Pertsch, Y. S. Kivshar, *Adv. Opt. Mater.* **2015**, *3*, 813.
[22] M. I. Shalaev, J. Sun, A. Tsukernik, A. Pandey, K. Nikolskiy, N. M. Litchinitser, *Nano Lett.* **2015**, *15*, 6261.
[23] W. Wan, J. Gao, X. Yang, *ACS Nano* **2016**, *10*, 10671.
[24] G. Zheng, H. Mühlenbernd, M. Kenney, G. Li, T. Zentgraf, S. Zhang, *Nat. Nanotechnol.* **2015**, *10*, 308.
[25] G. Hou, Z. Wang, Z. Lu, H. Song, J. Xu, K. Chen, *ACS Appl. Mater. Interfaces* **2020**, *12*, 56178.
[26] N. Yu, F. Aieta, P. Genevet, M. A. Kats, Z. Gaburro, F. Capasso, *Nano Lett.* **2012**, *12*, 6328.
[27] E. Karimi, S. A. Schulz, I. De Leon, H. Qassim, J. Upham, R. W. Boyd, *Light: Sci. Appl.* **2014**, *3*, e167.
[28] M. Mehmood, S. Mei, S. Hussain, K. Huang, S. Siew, L. Zhang, T. Zhang, X. Ling, H. Liu, J. Teng, *Adv. Mater.* **2016**, *28*, 2533.
[29] S. Sun, Z. Zhou, C. Zhang, Y. Gao, Z. Duan, S. Xiao, Q. Song, *ACS Nano* **2017**, *11*, 4445.
[30] L. Liu, X. Zhang, M. Kenney, X. Su, N. Xu, C. Ouyang, Y. Shi, J. Han, W. Zhang, S. Zhang, *Adv. Mater.* **2014**, *26*, 5031.
[31] K. Chen, Y. Feng, F. Monticone, J. Zhao, B. Zhu, T. Jiang, L. Zhang, Y. Kim, X. Ding, S. Zhang, *Adv. Mater.* **2017**, *29*, 1606422.
[32] N. Yu, P. Genevet, M. A. Kats, F. Aieta, J.-P. Tetienne, F. Capasso, Z. Gaburro, *Science* **2011**, *334*, 333.
[33] K. E. Chong, I. Staude, A. James, J. Dominguez, S. Liu, S. Campione, G. S. Subramania, T. S. Luk, M. Decker, D. N. Neshev, *Nano Lett.* **2015**, *15*, 5369.
[34] J. Kim, Y. Li, M. N. Miskiewicz, C. Oh, M. W. Kudenov, M. J. Escuti, *Optica* **2015**, *2*, 958.

[35] A. C. Overvig, S. Shrestha, S. C. Malek, M. Lu, A. Stein, C. Zheng, N. Yu, *Light: Sci. Appl.* **2019**, *8*, 92.
[36] Z. Ma, S. M. Hanham, P. Albella, B. Ng, H. T. Lu, Y. Gong, S. A. Maier, M. Hong, *ACS Photonics* **2016**, *3*, 1010.
[37] J. B. Mueller, N. A. Rubin, R. C. Devlin, B. Groever, F. Capasso, *Phys. Rev. Lett.* **2017**, *118*, 113901.
[38] W. Liu, H. Cheng, J. Tian, S. Chen, *Adv. Phys.: X* **2020**, *5*, 1742584.
[39] M. Pan, Y. Fu, M. Zheng, H. Chen, Y. Zang, H. Duan, Q. Li, M. Qiu, Y. Hu, *Light: Sci. Appl.* **2022**, *11*, 195.
[40] R. Fleury, D. L. Sounas, A. Alu, *Phys. Rev. Lett.* **2014**, *113*, 023903.
[41] S. Tang, X. Li, W. Pan, J. Zhou, T. Jiang, F. Ding, *Opt. Express* **2019**, *27*, 4281.
[42] Z.-L. Deng, G. Li, *Mater. Today Phys.* **2017**, *3*, 16.
[43] P. C. Wu, R. A. Pala, G. Kafaie Shirmanesh, W.-H. Cheng, R. Sokhoyan, M. Grajower, M. Z. Alam, D. Lee, H. A. Atwater, *Nat. Commun.* **2019**, *10*, 3654.
[44] X. Liu, X. Jia, M. Fischer, Z. Huang, D. R. Smith, *Nano Lett.* **2018**, *18*, 6181.
[45] X. Ni, Z. J. Wong, M. Mrejen, Y. Wang, X. Zhang, *Science* **2015**, *349*, 1310.
[46] J. Dixon, M. Lawrence, D. R. Barton III, J. Dionne, *Phys. Rev. Lett.* **2021**, *126*, 123201.
[47] X. Liu, Z. Huang, J. Zang, *Nano Lett.* **2020**, *20*, 8739.
[48] X. Chen, H. Zou, M. Su, L. Tang, C. Wang, S. Chen, C. Su, Y. Li, *Nanomaterials* **2021**, *11*, 1137.
[49] X. Zhang, R. Deng, F. Yang, C. Jiang, S. Xu, M. Li, *ACS Photonics* **2018**, *5*, 2997.
[50] D. Zhang, M. Ren, W. Wu, N. Gao, X. Yu, W. Cai, X. Zhang, J. Xu, *Opt. Lett.* **2018**, *43*, 267.
[51] Z. Wang, C. Dai, Z. Li, Z. Li, *Nano Lett.* **2022**, *22*, 2059.
[52] Z. Li, E. Palacios, S. Butun, K. Aydin, *Nano Lett.* **2015**, *15*, 1615.
[53] H. F. Ma, Y. Q. Liu, K. Luan, T. J. Cui, *Sci. Rep.* **2016**, *6*, 1.
[54] G. W. Milligan, M. C. Cooper, *J. Classif.* **1988**, *5*, 181.

